



HAL
open science

Numerical Modeling and Optimization of Thermal Stratification in Solar Hot Water Storage Tanks for Domestic Applications: CFD Study

Tarik Bouhal, Saïf Ed-Dîn Fertahi, Younes Agrouaz, Tarik El Rhafiki, Tarik Kousksou, Abdelmajid Jamil

► To cite this version:

Tarik Bouhal, Saïf Ed-Dîn Fertahi, Younes Agrouaz, Tarik El Rhafiki, Tarik Kousksou, et al.. Numerical Modeling and Optimization of Thermal Stratification in Solar Hot Water Storage Tanks for Domestic Applications: CFD Study. *Solar Energy*, 2017, 157, pp.441-455. 10.1016/j.solener.2017.08.061 . hal-02153535

HAL Id: hal-02153535

<https://univ-pau.hal.science/hal-02153535>

Submitted on 29 Apr 2024

HAL is a multi-disciplinary open access archive for the deposit and dissemination of scientific research documents, whether they are published or not. The documents may come from teaching and research institutions in France or abroad, or from public or private research centers.

L'archive ouverte pluridisciplinaire **HAL**, est destinée au dépôt et à la diffusion de documents scientifiques de niveau recherche, publiés ou non, émanant des établissements d'enseignement et de recherche français ou étrangers, des laboratoires publics ou privés.

Numerical modeling and optimization of thermal stratification in solar hot water storage tanks for domestic applications: CFD study

T. Bouhal^{a,b,*}, S. Fertahi^b, Y. Agrouaz^{a,b}, T. El Rhafiki^c, T. Kousksou^a, A. Jamil^b

^a Université de Pau et des Pays de l'Adour, Laboratoire des Sciences pour l'Ingénieur Appliquées à la Mécanique et au Génie Electrique (SIAME), IFR – A. Jules Ferry, 64000 Pau, France

^b École Supérieure de Technologie de Fès, Université Sidi Mohamed Ben Abdellah, Route d'Imouzzer BP 2427, Morocco

^c École Nationale Supérieure d'Arts et Métiers ENSAM, Université Moulay Ismail (U.M.I), Marjane II, BP-4024 Meknès Ismailia, Morocco

This study aims to assess the thermal stratification inside a standard hot water storage tank such an important device of solar water heaters. A number of flat plates with different titled positions are integrated inside a vertical tank prototype. The purpose of this investigation is to numerically study the impact of the flat plate positions within a vertical storage tank, which operates during the charging mode, on the thermal stratification and to conduct the possible performance enhancements to achieve. CFD numerical comparison between two configurations was carried out and performance parameters such as temperature evolution, Richardson number and stratification number were calculated. It was shown that thermal stratification inside the storage tank is depending on the flat plate's positions. Thus, increasing flat plates in different positions inside the storage tank does not establish a suitable thermal stratification. Therefore, a superior thermal performance was achieved for the flat plate which is maintained at the middle height of the storage tank. Also, it was found that flat plate's integration at different angles improves the thermocline structure development.

1. Introduction

Thermal stratification in solar storage tanks has a major effect on the thermal performance of a solar water heating system.

Preserving the thermocline stability and stratification are an effective solutions to enhance the efficiency of thermal storage devices strained with lag time between the production and the demand, or for an irregular available energy source. Naturally, sensible heat storage is widely used in such systems thanks to their simplicity and low cost especially in solar energy, air conditioning and refrigeration applications. Water storage tanks offer an attractive options for those systems due to the low cost, the abundance and also the good water thermal properties.

A good thermal storage tank performance and a substantial increase in the total efficiency may be achieved by improving the thermal stratification degree which has been the subject of various numerical studies. For instance, [Bonanos and Votyakov \(2016\)](#) realized a sensitivity analysis for thermocline thermal storage tank design. They find that the thermocline is sensitive to the tank height and the filler material properties. The properties of the fluid, the particle size, void fraction and charging times have a secondary influence, whereas the

viscosity of the heat transfer fluid has a negligible effect on the thermocline thickness. Moreover, [Erdemir and Altuntop \(2016\)](#) analyzed the thermal stratification of vertical mantled hot water tank with four obstacles. They found that placing the obstacle inside the inner tank in vertical mantled hot water tanks improve the thermal stratification. The best thermal stratification was obtained between $Y = 200$ mm and $Y = 300$ mm the distance from the tank bottom. Recently, [Fan and Furbo \(2012\)](#) presented numerical studies of thermal stratification established by standby heat loss from a vertical cylindrical hot water tank. They got a generalized equation that was implemented in a design program of an existing tank optimization in order to estimate its thermal performances.

[Gandhi et al. \(2013\)](#) assessed the flow patterns and temperature in centrally heated cylindrical tank and investigated the effect of passive devices like draft tube, fins and aspect ratio on stratification. Their results show that using fins of suitable size with its appropriate positions severely reduces mixing time and stratification. A good agreement was achieved between the experimental and the predicted values of heat transfer coefficient. Also, [García-Marí et al. \(2013\)](#) developed a new inlet device that increase thermal stratification in a hot water storage tank during charging based on two water inlet devices: a

* Corresponding author at: Université de Pau et des Pays de l'Adour, Laboratoire des Sciences pour l'Ingénieur Appliquées à la Mécanique et au Génie Electrique (SIAME), IFR – A. Jules Ferry, 64000 Pau, France.

E-mail address: bouhal.tarik12@gmail.com (T. Bouhal).

Nomenclature

Symbols

v_{in}	inlet velocity [m/s]
T_{ini}	initial temperature [K]
T_{in}	inlet temperature [K]
H	length of the tank [m]
h	location of the plate [m]
d	diameter of the plate [m]
D	diameter of the tank [m]
α	tilt angle [°]
Q_{in}	inlet mass flow rate [kg/s]
Q_{out}	outlet mass flow rate [kg/s]
u	horizontal velocity [m/s]
v	vertical velocity [m/s]

ρ	density [kg/m ³]
β	thermal expansion coefficient [1/K]
μ	dynamic viscosity [Pa·s]
C_p	specific heat capacity [J/K·kg]
T	temperature [K]
λ	thermal conductivity [W/K·m]
Ri	Richardson number
T_{top}	tank top temperature [K]
T_{bottom}	tank bottom temperature [K]

Abbreviations

CFD	Computational Fluid Dynamics
Str	Stratification number

conventional inlet elbow and a sintered bronze conical diffuser. The results show that the use of conical diffuser for the hot water inlet promotes thermal stratification of the water. Furthermore, Göppert et al. (2009) introduced a new computation method for stratification pipes of solar storage tanks making the effects estimation of the constructive and the determination of the individual fluid flows changes possible. A good agreement was found for a simple charge system using comparison with CFD. Joseph et al. (2016) studied the effect of insulation thickness on pressure evolution and thermal stratification in a cryogenic tank. The results show that the reduction in insulation thickness can increase in pressure rise and in stratified mass when tank is insulated with lower insulation thickness. In addition, Kong et al. (2016) performed a CFD simulations of thermal stratification inside cylinder with openings in a heat storage water tank. They conclude that cylinder insides the tank plays a role of uniform diffuser, so that the water in the tank is forming thermal stratification.

From the literature survey, draw-offs and loading hot water can seriously affect thermal stratification and the overall efficiency of small solar domestic storage tanks, as it was detailed in the recent work of Jordan and Furbo (2005). Besides, the effect of a porous manifold on thermal stratification inside a liquid storage tank was investigated through the work conducted by Yee and Lai (2001). Moreover, using different inlet stratifiers would severely assign thermal stratification Dragsted et al. (2017). Furthermore, Wang and Davidson (2015) proposed a permeability selection of a porous tube thermal stratification manifold so as to enhance its performance, besides finding an optimal operating point. Last but not least, Brown and Lai (2011) carried out experimental investigation to enhanced the thermal stratification within a liquid storage tank which integrates a porous manifold.

Brown and Lai (2011) studied experimentally enhanced thermal stratification in a liquid storage tank with a porous manifold and its effectiveness. Furthermore, Wang and Davidson (2017) investigated the performance of a rigid porous-tube stratification manifold in comparison to an inlet pipe. In addition, Haller et al. (2010) presented a new method for the calculation of a stratification efficiency of thermal energy storage processes independently from storage heat losses. Brown and Lai (2011) performed numerical analysis of single tank thermocline system with different HTFs to investigate the performance of single-tank thermocline storage systems for CSP plants.

Several recent studies which aim to assess and to optimize hot water storage tanks energy performance are carried out through CFD simulations. A Cylinder with Openings (ICO) was integrated inside the studied tank, and Allouche et al. (2016) validated a CFD model used to simulate the heat transfer in a tubes-in-tank PCM storage unit. Moreover, Kassemi and Kartuzova (2016) studied the effect of interfacial turbulence and accommodation coefficient on CFD predictions of pressurization and pressure control in a cryogenic storage tank.

Furthermore, Cascetta et al. (2016) compared their CFD simulations to the experimental investigations of a packed-bed thermal energy storage system. Recently, Miana et al. (2011) worked on the enhancement of the thermal design of bitumen emulsion tanks by Scale Analysis. CFD models and experimental tests were used for this purpose assessment. Besides, N.H.S. Tay et al. (2012) conducted experimental validation of CFD model for tubes in a phase change thermal energy storage system in order to increase its energy storage performance. Meng and Zhang (2017) performed experimental and numerical investigation of a tube-in-tank latent thermal energy storage unit using composite PCM. Last but not least, Kaloudis et al. (2016) launched numerical simulations of constant-influx gravity currents in confined spaces. The thermal storage tanks were a case of their application.

Nash et al. (2017) modeled under three operation modes a dynamic sensible thermal energy storage inside a tank equipped with an immersed coil heat exchanger. In addition to this, Wang et al. (2017a) investigated the thermal stratification of a dynamic hot water storage tank with a novel inlet through experimental and numerical research methodologies. Jin et al. (2017) investigated experimentally a Novel Multi-Tank Thermal Energy Storage System for Solar-powered Air Conditioning application. Moreover, Rahman et al. (2016) conducted a performance modeling and a parametric study of a stratified water thermal storage tank.

Gasque et al. (2015) studied the influence of inner lining material on thermal stratification in a hot water storage tank. Furthermore, Saghii and Lakzian (2017) optimized a rectangular storage tanks used for the sloshing phenomena through an entropy generation minimization. Adolfo et al. (2014) analyzed numerically a thermal storage tank which is used as a part of a 20 kW for a Solar/gas Adsorption Air Conditioning System (ACS). Recently, Ali et al. (2015) studied the effect of a thermal fluid and the design of a thermal energy storage tank in Solar Energy Applications (SEA). Also, Reddy et al. (2017) investigated the performance of single-tank thermocline storage systems for CSP plants, and Votyakov and Bonanos (2015) developed an algebraic model for thermal storage tank thermoclines using filler materials.

Investigating the obstacle's effect on thermal stratification in hot water storage tanks was presented in the work of Altuntop et al. (2005), because of its importance to define its energy performance. In addition to this, Gyüre and János (2003) have characterized a stratified flow over asymmetric and double bell-shaped obstacles. Moreover, Gross et al. (1987) conducted several numerical simulations in order to describe the dispersion over and around a steep obstacle intended to vary thermal stratification. An other study was performed by Wang et al. (2017b), it has investigated a novel equalizer structure designed to enhance thermal stratification characteristics within a dynamic hot water storage tank.

As we can see, thermal stratification is affected by many factors such

as the aspect ratio of the tank (height to diameter), heat losses to the surroundings and the mixing due to the inlet and outlet streams. Through the current study, another technique which aims to enhance the thermal stratification by the integration of a flat plate inside the solar storage tank is conducted. Hence, this paper focuses on the effect of the flat plate's positions and orientations on the thermal performance for two storage tanks configurations. The CFD commercial code Fluent 15 was used in order to carry out the numerical simulations and also to explain the numerical observations and results.

2. Context of the study

The models representing the thermal stratification in hot water tanks treat in their majority the case of a vertical tank fed out with cold water from the bottom and providing hot water from the top according to load profiles. The stratification is modelled by dividing the tank into sufficiently fine horizontal layers for numerical stability reasons. For each layer, the energy and mass equations were established. The resolution of the total system provides the temperatures characterizing the tank layer's according to water loading profile, the required heating energy (electricity at night and solar supplement or gas during the day consumption)....

Hot water production constitutes one of solar energy's privileged applications in the buildings. This is due to the nature of the need: hot water temperature (between 45 and 60 °C), weak variation needs during the year. In addition to the solar collectors, the essential component of a solar water heating system is the hot water storage tank (Fig. 1). The energy stored inside the tank is increased, if the stratification is well improved. Consequently, the aim of the current study is to understand the thermal behaviour of the storage tank by conducting a CFD parametric study on a standard storage tank as schematically presented in Fig. 1.

2.1. Definition of schematic configurations

In the present paper, a numerical investigation was conducted on two thermal storage tank configurations as presented schematically in Figs. 2 and 3.

Fig. 2 presents the geometric model of the solar hot water storage tank fit with a metal flat plate sufficiently thin located at a height of h with a diameter d . The physical model for charging process in cylindrical tank consists of an outlet and an inlet ports in the right side of the wall tank. The cold water inlet is from the bottom of the tank and the hot water outlet is from its top as presented in Fig. 2. The inlet supply

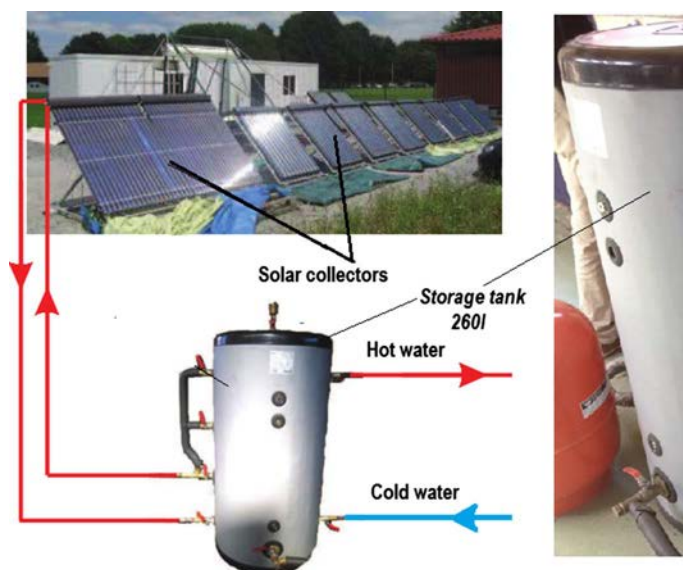


Fig. 1. In situ picture of the storage tank subjected to the numerical studies.

has uniform velocity $v_{in} = 0.1694 \text{ m s}^{-1}$ and temperature of $T_{in} = 15 \text{ }^\circ\text{C}$. The external walls and flat plate are kept adiabatic. 2D unsteady flow models in charging mode were built in Fluent CFD commercial software. It was used as the CFD solver and the grid generator respectively.

Seven different storage tank configurations were considered with flat plates placed in three positions (Bottom, Middle and Top) inside the vertical standard hot water tank. Thus, the performed configurations are: 1-Bottom, 1-Middle, 1-Top, 2-Bottom-Middle, 2-Middle-Top, 2-Bottom-Top and 3 flat plates completely integrated inside the storage tank as presented in Fig. 2. The aim is to study the effect of flat plate's positions on thermal stratification inside the standard storage tank.

Fig. 3 illustrates the second configuration of the schematic storage tank. In this case, the outlet and inlet nozzles are located at the centre top and bottom surfaces of the storage tank respectively. The storage tank is equipped with a metal flat plate also sufficiently thin located at mid-height with a diameter d . The water tank dimensions are illustrated in Fig. 3. The inlet flow passes from the area between the main tank and the flat plate. This configuration was designed to reduce the jet flow which causes mixing process. The hot water flow is extracted from the highest the tanks point to make sure the outlet temperature is maximum. Simulations were performed with initial and inlet temperatures of 50 °C and 15 °C respectively for a uniform velocity of 0.1694 m s⁻¹. Also, the external walls and flat plate are maintained adiabatic.

In this configuration, the storage tank contains a flat plate placed in different orientations quantified by the angle α which varies from 0 to π ($0 \leq \alpha \leq \pi$) as presented in Fig. 3. The main purpose is to study the impact of flat plate's angle on thermal stratification inside the vertical storage tank.

An optimized adaptive mesh refinement solution is used in order to better predict the internal flow field behaviour, so that a finer mesh was applied to the whole flow field and for predicting correctly the features of the flow. The CFD code was accounting for a two-dimensional effects. Indeed, a 2D section passing throughout the half of the tank was modeled since the tank's geometry was symmetric and all the results in term of temperature contours and streamlines were plotted on it. Working on a 2D section decreased the computational time and it was a suitable approach to model the cycles of charging and discharging which occur during water consumption.

The main objective of the present study is to investigate the thermal flow fields evolution during the charging operation mode and the process of thermal stratification establishing inside the studied storage tank.

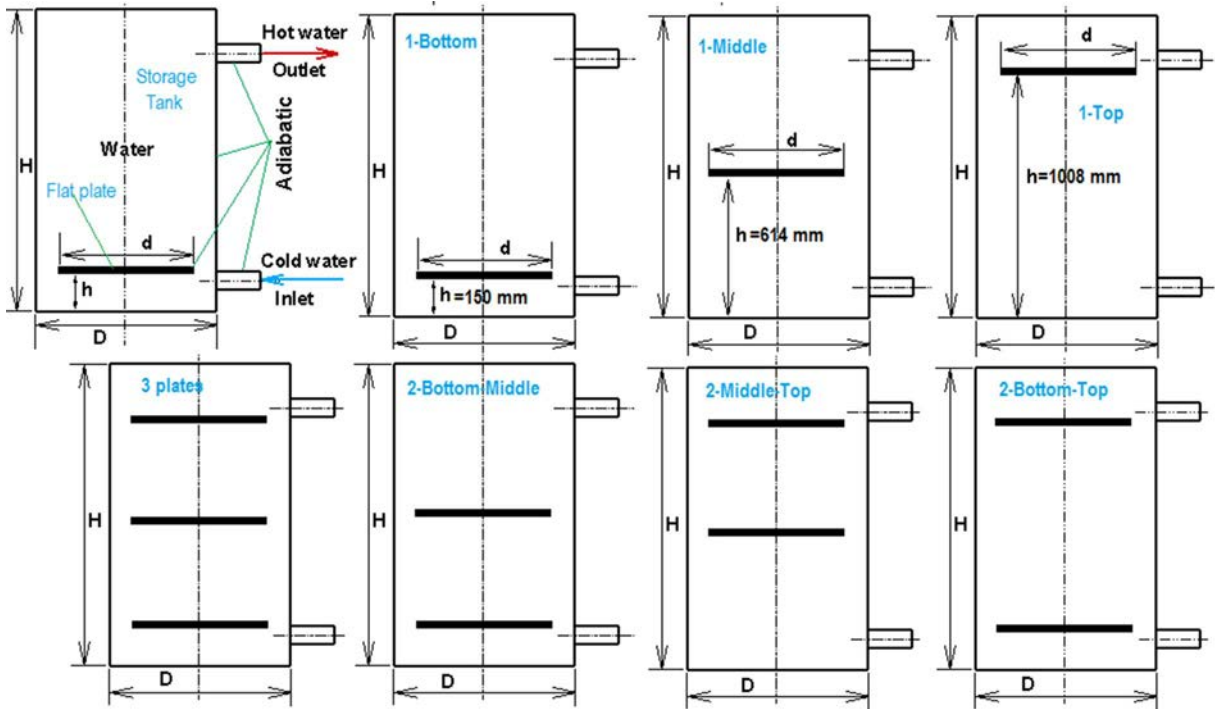


Fig. 2. Schematic configurations of the storage tank with different flat plat's positions.

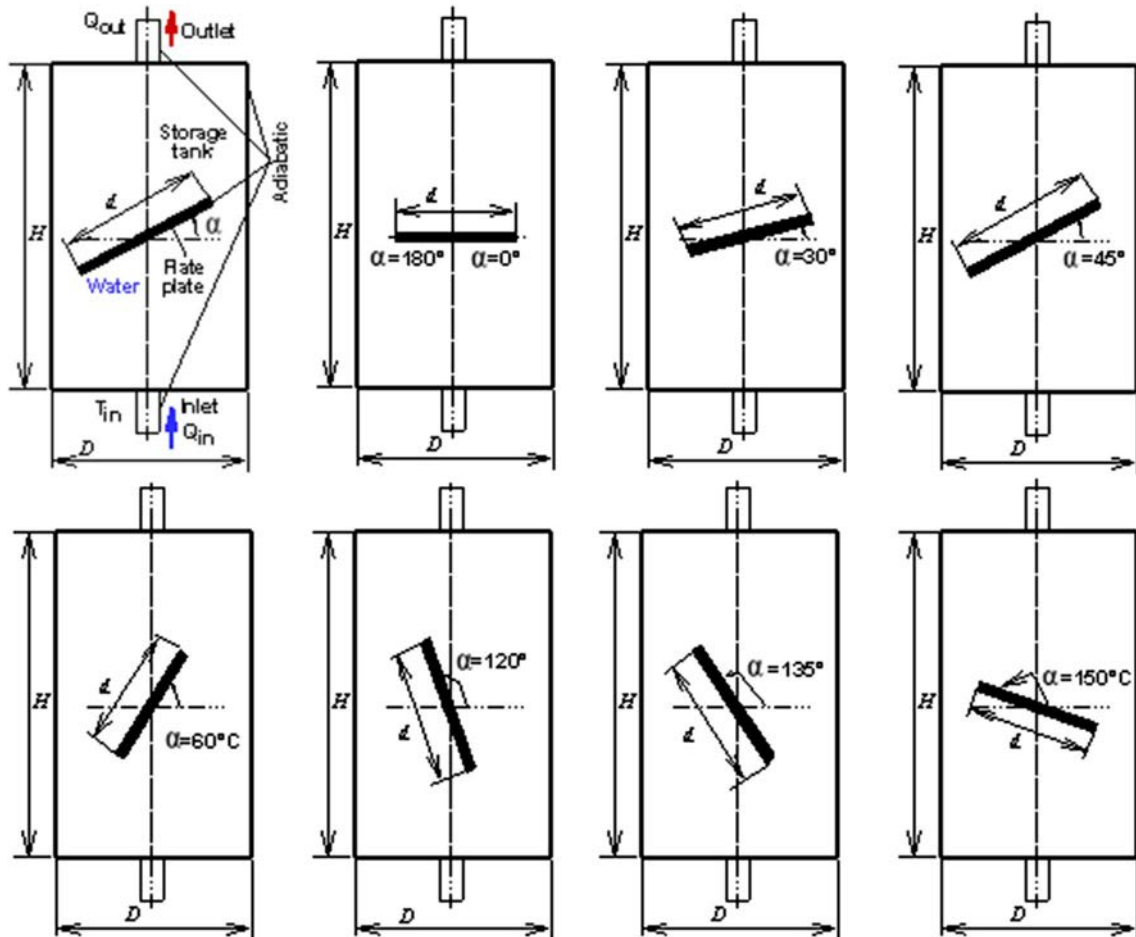


Fig. 3. Schematic configurations of the storage tank with different flat plat's orientations.

2.2. Mathematical formulation

Unsteady two-dimensional flow models of heat transfer inside a standard storage tank were governed by the general following assumptions:

1. The working fluid is incompressible.
2. The thermophysical properties of the liquid are constant except for the density variation with temperature, which is responsible for the generation of thermal buoyancy, for using the Boussinesq approximation.
3. The liquid is Newtonian.
4. The viscous dissipation is negligible.
5. Fluid motion is laminar and two-dimensional.

The energy and Navier-Stokes equations in two-dimensional form were used to solve the transient hydrodynamic and thermal fields. Therefore, the resulting governing equations with consideration of gravity effect can be written as follows taking into account the foregoing assumptions:

2.2.1. Continuity equation

The continuity equation is formulated in the following manner in cylindrical co-ordinate system:

$$\nabla \cdot \mathbf{u} = 0 \quad (1)$$

Eq. (1) can be applied to incompressible fluids, meaning that $\rho(r,z,t) = \text{constant}$. Where t is time, the z and r mean the vertical and the radial directions respectively.

2.2.2. Momentum equation

The following Eq. (2) is the representation of the momentum equations in cylindrical co-ordinate system.

$$\rho \frac{\partial \mathbf{u}}{\partial t} + (\rho \mathbf{u} \cdot \nabla) \mathbf{u} = -\nabla p + \nabla \cdot \tau - \rho \beta (T - T_{ref}) g \quad (2)$$

where p is the static pressure, τ is the stress tensor (described below), $\rho \beta (T - T_{ref}) g$ is the gravitational body force.

The stress tensor τ is given by Eq. (3):

$$\tau = \mu [(\nabla \mathbf{u} + \nabla \mathbf{u}^T)] \quad (3)$$

where μ is the molecular viscosity.

2.2.3. Heat transport equation

The 2D diffusion/convection equation is solved to calculate the temperature field (Eq. (4)):

$$\rho C_p \frac{\partial T}{\partial t} + \rho C_p \mathbf{u} \cdot \nabla T = \nabla \cdot (\lambda \nabla T) \quad (4)$$

where C_p is the specific heat of the water at constant pressure and λ is the laminar thermal conductivity of the fluid.

2.3. Mesh grid

A structured grids was used and the final mesh was composed of about 127,000–140,000 elements depending on the considered storage tank configuration. The cells close to outlet and inlet apertures and walls are small enough to capture the complex flow structure as presented in Fig. 4.

2.4. Boundary conditions

The resolution of the equations governing the heat transfer inside the storage tank requires the incorporation of boundary conditions for both configurations and for each dependent variable (see Fig. 3). The boundary conditions of the studied configurations and their geometrical

dimensions are presented schematically in Fig. 5.

Water was used as a working fluid filling the storage tank. The pressure inlet boundary conditions applied to the fluid flow and the outlet of the water storage tank is assigned to be a pressure outlet boundary condition. Adiabatic thermal condition is applied for the storage tank walls by setting a zero heat flux at the wall surfaces. No-slip condition is applied at all solid surface walls, i.e., the velocity of the fluid at the wall is zero. That is, the water fluid at the walls is not moving. The condition prescribes:

$$u = v = 0 \quad (5)$$

The zero heat flux boundary condition is assigned to every bottom, top and side tank walls, assuming the surface walls are perfectly insulated from the outside. According to Fig. 3, the equations for this boundary condition are as follows:

- Configuration (a)

– At the adiabatic top and bottom surfaces:

$$u = v = 0 \text{ and } \frac{\partial T}{\partial r} = 0 \text{ at } -\frac{D}{2} \leq r \leq \frac{D}{2}, z = 0 \text{ and } z = H \quad (6)$$

– At the adiabatic side walls:

$$u = v = 0 \text{ and } \frac{\partial T}{\partial r} = 0 \text{ at } 0 \leq z \leq H \text{ and } r = \frac{D}{2} \quad (7)$$

$$u = v = 0 \text{ and } \frac{\partial T}{\partial r} = 0 \text{ at } 0 \leq z \leq e - \frac{a}{2}, e + \frac{a}{2} \leq z \leq H - e' - \frac{a}{2}, H - e' + \frac{a}{2} \leq z \leq H \text{ and } r = \frac{D}{2} \quad (8)$$

– At the adiabatic flat plate:

$$u = v = 0 \text{ and } \frac{\partial T}{\partial r} = 0 \text{ at } z = h \text{ and } -\frac{d}{2} \leq r \leq \frac{d}{2} \quad (9)$$

- Configuration (b)

– At the adiabatic top and bottom surfaces:

$$u = v = 0 \text{ and } \frac{\partial T}{\partial r} = 0 \text{ at } -\frac{D}{2} \leq r \leq -\frac{b}{2}, \frac{b}{2} \leq r \leq \frac{D}{2}, z = 0 \text{ and } z = H \quad (10)$$

– At the adiabatic side walls:

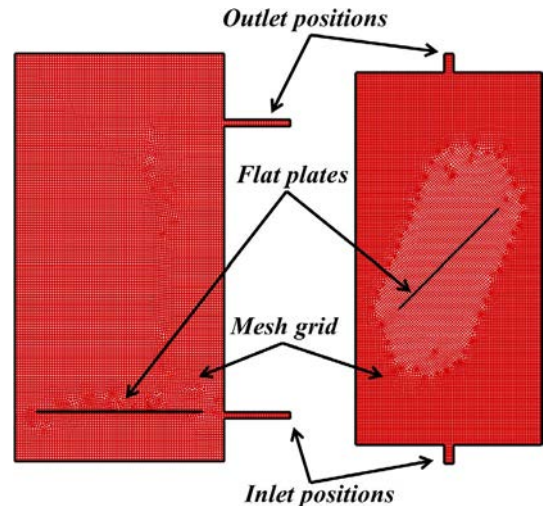


Fig. 4. Structured mesh grid of the storage tank for both configurations.

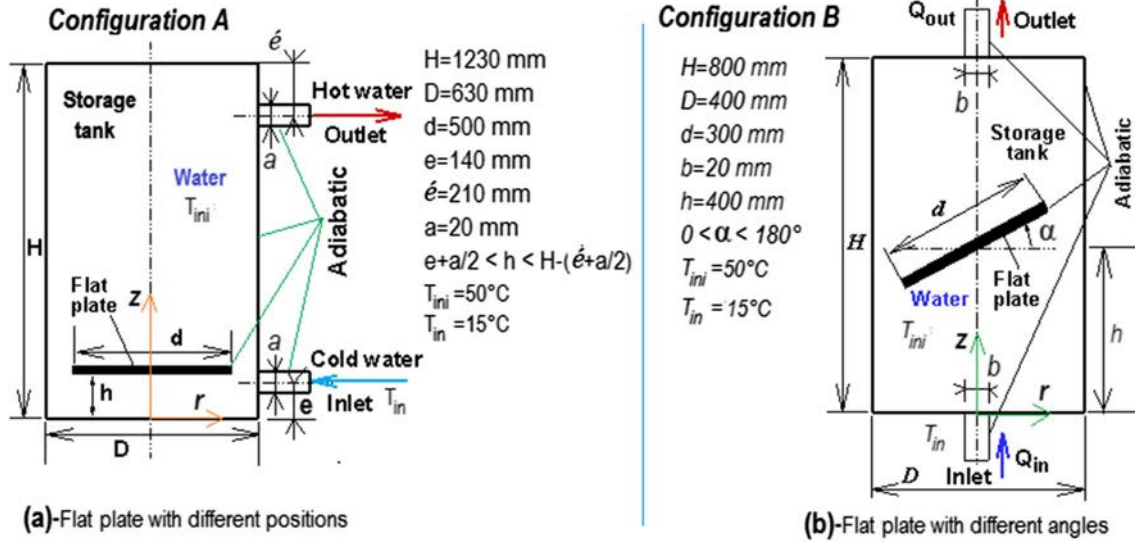


Fig. 5. Boundary conditions for both configurations.

$$u = v = 0 \text{ and } \frac{\partial T}{\partial r} = 0 \text{ at } 0 \leq z \leq H \text{ and } r = \frac{D}{2} \quad (11)$$

– At the adiabatic flat plate:

$$u = v = 0 \text{ and } \frac{\partial T}{\partial r} = 0 \text{ at } z = \frac{H}{2} \text{ and } -\frac{d}{2} \cos \alpha \leq r \leq \frac{d}{2} \cos \alpha, \alpha \in [0, \pi] \quad (12)$$

3. CFD code validation

Zachár et al. (2003) tested a transparent tank which allowed them to visualize the stratification when dye is injected into water. Fig. 6 represents a two-dimensional section of the experimental tank on which its dimensions are indicated. The temperature inside the tank was measured by a thermocouple tree on which a series of 20 sensors were stuck. The thermocouple tree is located half way between the symmetry axis and the wall tank. Zachár et al. (2003) validated their experimental measurements through the development of their own house program, and also by using the CFX commercial code. The commercial code Fluent 15 was used to reproduce the results presented in the study of Zachár et al. (2003). The validation study is based on the comparison of the temperature evolution in the axial direction inside the tank as presented in Fig. 6.

3.1. Experimental section

The cylindrical tank that is the subject of the experimental study has an internal diameter of 400 mm, a length of 800 mm. The part at which the charging and the discharging operations are carried out is located in the middle top and bottom sides of the tank. The diameter of these nozzles is 200 mm. A very thin plate with 300 mm in diameter is located in the lower zone of the tank. It is 40 mm apart from the injection nozzle. Its role is to decrease the flow velocity coming from the inlet section and thereafter to improve the stratification inside the tank. The operating conditions used for the validation are an imposed flow $Q_{in} = 0.26 \text{ kg/s}$ at the inlet nozzle. The tank walls are insulated and the map of acquisition is connected to a computer and ensures the recording of the temperature at the end of each 10 s.

3.2. CFD model

Transient CFD simulations were performed to validate the numerical results against experimental measurements. The SIMPLE algorithm is used for the pressure-velocity coupling. The second order scheme and the first Upwind method are used for the discretization of pressure and the momentum/energy equations respectively. A time step in the range of 10^{-3} – 10^{-4} and a cell size of 4 mm are found to be appropriate and are used in the calculations. The flow regime is supposed to be laminar because of the low flow in the charge discharge cases which were studied during the experiment. The transient simulation starts from a tank with a uniform temperature of 40 °C. A zero velocity field is assumed at the start of all the simulations. The numerical solution is supposed to be convergent when the scaled residuals for the continuity, the momentum and the energy equations are less than 10^{-4} , 10^{-4} and 10^{-8} respectively. A parallel calculation was launched on a Z600 workstation (16 CPU, 32 Go RAM). The computational time lasts 9 h as an average with a time step value of 10^{-3} s.

Fig. 8 presents the axial position effect on the variation of the dimensionless fluid temperature T^* which is defined as follows:

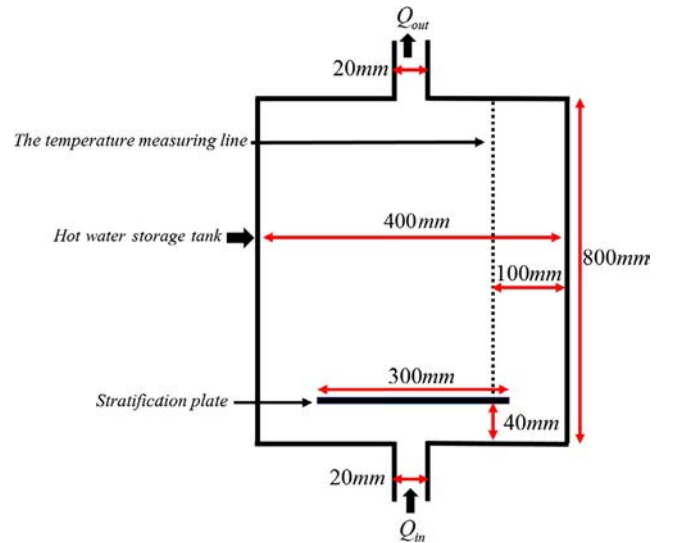


Fig. 6. A two-dimensional section of the experimental tank illustrating its dimensions.

$$T^* = \frac{T - T_{in}}{T_{ini} - T_{in}} \quad (13)$$

A good agreement was found between our numerical and the experimental results. We distinguish between three temperature evolution zones. The first zone is represented by the first quarter of the tank which extends over 200 mm. The temperature difference $T - T_{in}$ is very important, which means that the ramp curve of $z = fct(T^*)$ is important too. The difference in temperature over the second quarter which extends over 135 mm (from 0.2 cm to 0.35 cm) is less important. Indeed, the dimensionless temperature varies between 0.1 and 0.9. The degree of stratification is average. For the last two remaining zones $0.35 \text{ cm} < z < 0.8 \text{ cm}$, the energy stored inside the tank is maximal since the dimensionless temperature is equal to 1. (Lack of stratification in these two zones).

Fig. 7 presents the effect of injecting cold water at 20 °C on the static temperature contours evolution between 20 s and 180 s. They visualize the effect of the charge and discharge operations on the thermal stratification layers.

The effect of different vertical positions on the dimensionless

temperature T^* is shown in Fig. 8. This figure illustrates the effect of injecting cold water at 20 °C on the static temperature contours evolution particularly in the time interval [20 s; 180 s].

The initial hot temperature decreases due to the injection of cold water from the lower nozzle. The magnitude of the dimensionless temperature is minimal as well as concentrated at time $t = 80 \text{ s}$ around 0.8 and 1 compared to the other instants recorded. This result is independent of the effect of the position, because the initial hot water is not yet mixed with the cold water charged. Subsequently, the extension of the dimensionless temperature increases and occupies a larger interval [0.05; 0.95] from time $t = 120 \text{ s}$ for a position $H = 500 \text{ mm}$ of the tank.

Values of the experimental dimensionless temperature measured by Zachár et al. (2003), our numerical results, as well as the relative errors are presented in Table 1. A slight relative errors are observed which proves that our simulation results are in a good agreement with the experimental results carried out by Zachár et al. (2003).

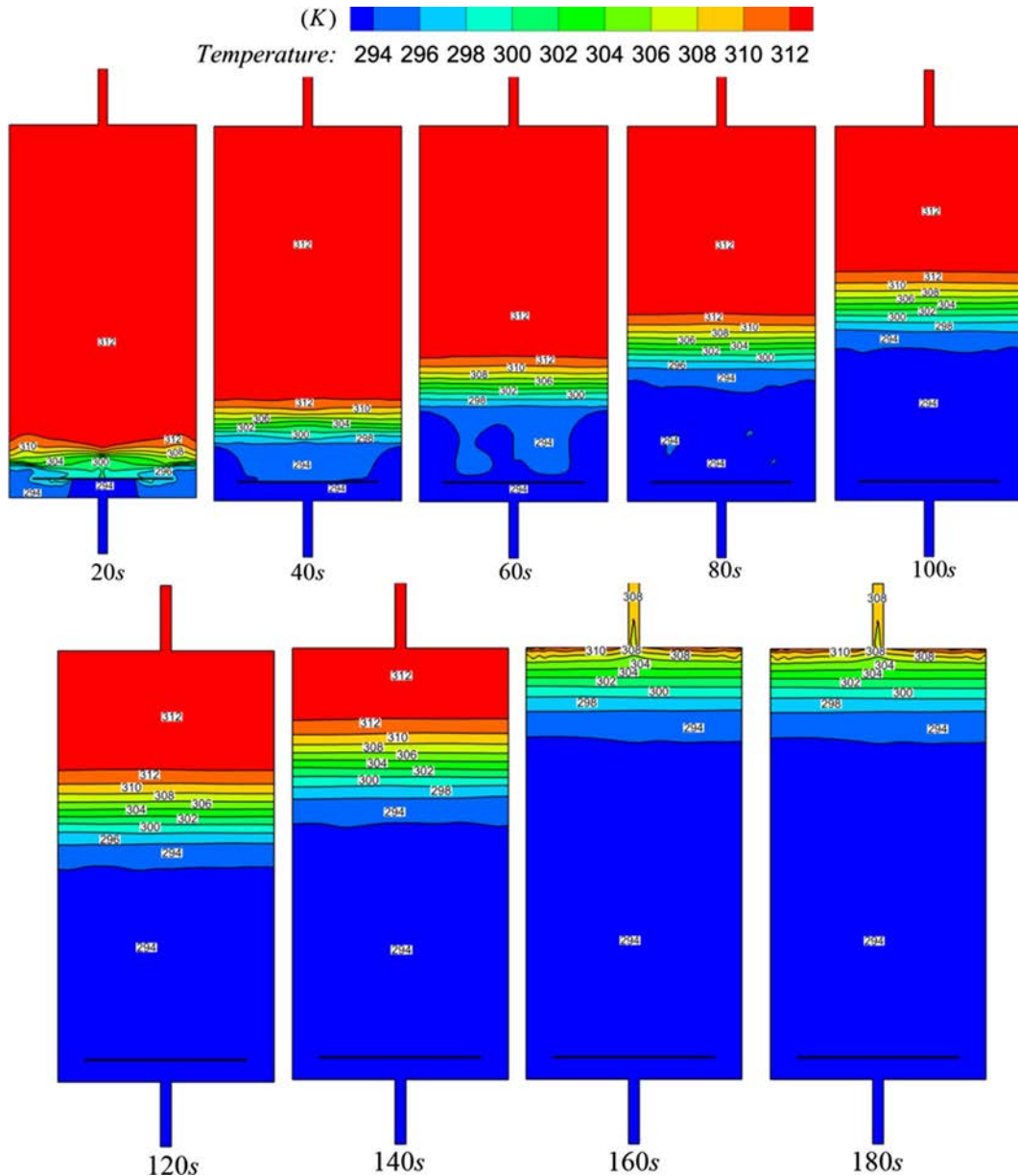


Fig. 7. The effect of injecting cold water at 20 °C on the evolution of the static temperature contours between 20 s and 180 s.

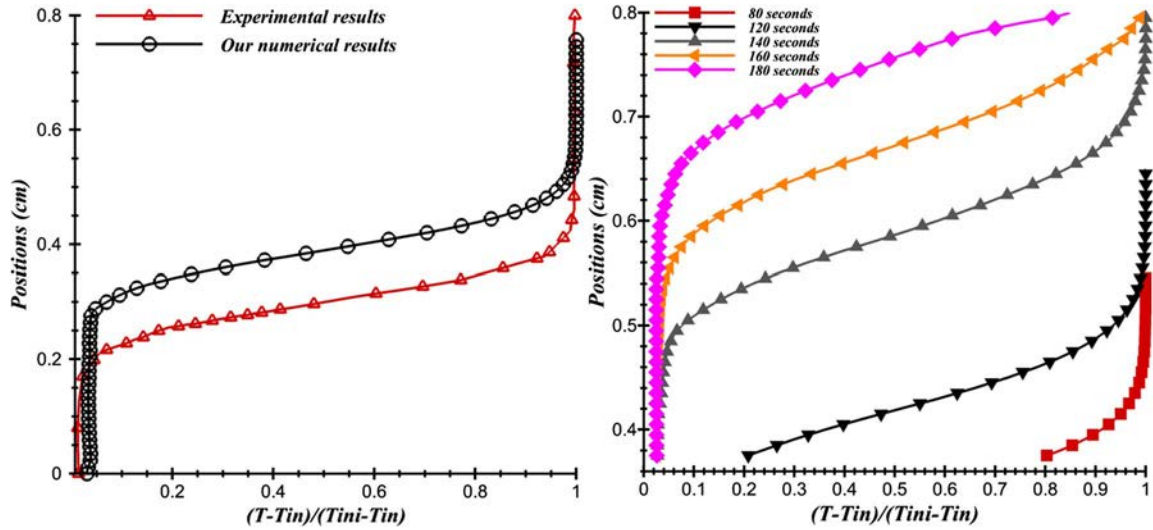


Fig. 8. Validation curve: The evolution of the dimensionless temperature along the tank height.

Table 1

Comparison between the numerical dimensionless temperatures and the relative error's evaluation.

Experimental results		Our numerical results		Relative error (%)
$\frac{T - T_{in}}{T_{ini} - T_{in}}$	Positions (cm)	$\frac{T - T_{in}}{T_{ini} - T_{in}}$	Positions (cm)	
0.13	0.24	0.13	0.32	0
0.137	0.24	0.131	0.32	4.37
0.2	0.25	0.2	0.34	0
0.27	0.26	0.27	0.35	0
0.37	0.28	0.37	0.37	0
0.54	0.3	0.54	0.39	0
0.69	0.32	0.68	0.41	1,44
0.84	0.35	0.83	0.445	1,19
0.91	0.37	0.91	0.45	0
0.98	0.41	0.99	0.49	1,02
0.99	0.52	0.99	0.52	0
1	0.55	0.99	0.55	1
1	0.55	1	0.55	0

4. Results and discussion

In the present study, a set of numerical simulations were performed to predict the performance of stratification inside a storage tank. As previously described, two configurations were used: configuration A with a flat plate placed at different positions while the configuration B represents the flat plate oriented at various α inclinations. The flat plates effect positions on thermal stratification was investigated. Thus, a two dimensional section of water temperature contours and streamlines, Richardson number, Stratification number of the tank, average and outlet temperature were used as indicators to determine the thermal stratification efficiency.

4.1. Temperature contours and streamlines

4.1.1. Configuration A with different positions

The temperature stratification inside the storage tank is affected by several factors. Therefore, the flowing section illustrates the effect of flat plates placed at different tank heights as well as their orientations on the temperature distribution inside the tank and the mixing behaviour at different time histories.

Fig. 9 describes the evolution of water temperature contours during

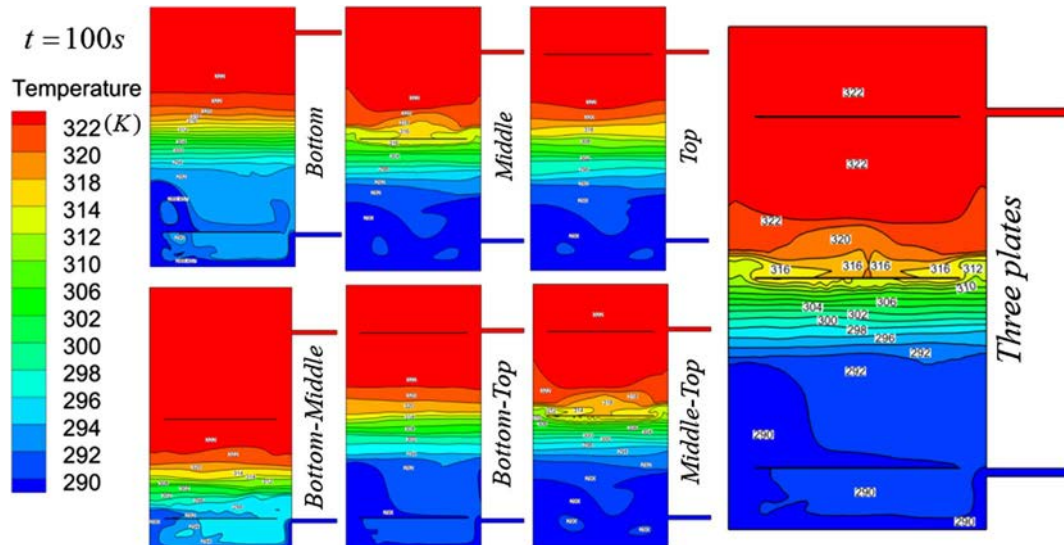


Fig. 9. Effect of flat plate at different positions on temperature contours (Configuration A).

the dynamic operation for different flat plates ranging: bottom, middle and top at $t = 100$ s. Simulation data are represented on the (r,z) plane and the tank height and diameter are fixed and have values of 1230 mm and 630 mm respectively to provide the required effect of flat plates integration. For all the performed simulations, the transient flow behavior especially the thermocline development and the accompanying entrainment mechanisms were presented. During the charging process, the collision of the incoming cold jet with the bottom layers produces vortex near the inlet port. The cold water with heavy density falls down dragging simultaneously the upper-layer water into the bottom. Due to buoyancy effect, the dragged-down filament rises up and diffuses amongst the fluid layers causing additional convection motion. These unbalanced forces of gravity and inhomogeneous penetration contribute to the enhancement of mixing which may extend to include most of the tank volume. As time progresses, the mixing zone widens continuously and the thermocline region tends to migrate from the bottom to the top of the tank. Through the graphs of isotherms fields. This phenomenon is clearly apparent for all flat plate's positions configurations at $t = 100$ s where the uniform region is taking over more than the half of the tank while the stratified one at the top becomes much thinner and thus results in a well-mixed tank.

Concerning the dynamic field represented by the contours of streamlines in Fig. 10. The flat plate are placed in three different status, i.e. in the bottom, middle and top positions inside the tank. For every case, it is assumed again that the cold fluid is charged from the bottom and it is loaded from the top outlet. As the hot fluid flow is initiated through the bottom port inlet, the tank cold fluid adjacent to the interface of the flat plate is progressively heated and flows upward due to the buoyancy force. The uprising warm fluid in the tank around the vicinity of the tank wall impinges to the top horizontal wall and turns towards the centerline of the tank and pushes the cold fluid to drop down around the centerline. Hence, a recirculation zone is formed at the bottom and top regions of the tank as may be seen in Fig. 10. As time passes, the hot water at the top region is replaced with the warmer water, and pushes down the previously hot fluid layer, causing the formation of a stable thermal stratification. The lower part of the tank is occupied with an almost stagnant cold fluid.

Comparing streamlines for the three cases shown in Fig. 10, we notice the appearance of a single circulation zone extends along the tank's diameter above the flat plate when it's placed at the bottom of the tank. The flow is oriented towards the outlet. As a result the plate

positioned at the bottom does not contribute enough to improve the thickness of the thermocline. Thus, the storing time of the stored hot water is not improved because of the inappropriate orientation of the streamlines.

By placing the flat plate in the middle, we observe the development of two rotating lobes. The first lobe at the tank bottom and the second lobe at the exit nozzle. Moreover, a set of thermoclines appeared on both sides of the plate placed in the middle. From Fig. 10, we notice that the storing time of the hot water is improved compared to the bottom configuration.

The zone at the bottom is occupied by a volume of water of low temperature (290 K) characterized a single large lobe which extends along the diameter of the tank since the flat plate is located at the top tank. Another circulation area occupies the volume above the plate. It is disturbed by rising streamlines from the bottom and enters through the ends of the plate.

Concerning the integration of two flat plates in bottom-middle inside the storage tank. A large volume of hot water above the middle position enters in recirculation following the introduction of lukewarm water from the ends. This configuration maximizes the storing time of the hot water through the reduction of the mixture.

In bottom-top configuration, the streamlines shape's which are developed in the middle of the tank are similar to those of the bottom, a configuration where the energy previously stored is damaged by the injection of cold water coming from the bottom nozzle.

The middle-top is characterized by the development of three circulation zones at the bottom, middle and top. The overall structure of the flow is disturbed and the range of the thermocline is less important than that of the bottom-top configuration.

Regarding three flat plates case, two circulation zones appear and are symmetrical to the axis of the tank. Two other zones appear along the plate in the bottom position. The range of the thermocline of this configuration is almost similar to that observed in the middle-top configuration.

For all configurations, we concluded that placing the flat plate around bottom position of the tank, the fluid on the upper part of the tank has a higher temperature at the same time and thermal stratification is reached over a higher section in the tank, while by placing flat plate around the bottom section of the tank, the maximum fluid temperature in the upper part of the tank is much lower than the two other cases and thermal stratification is created in much lower height of tank.

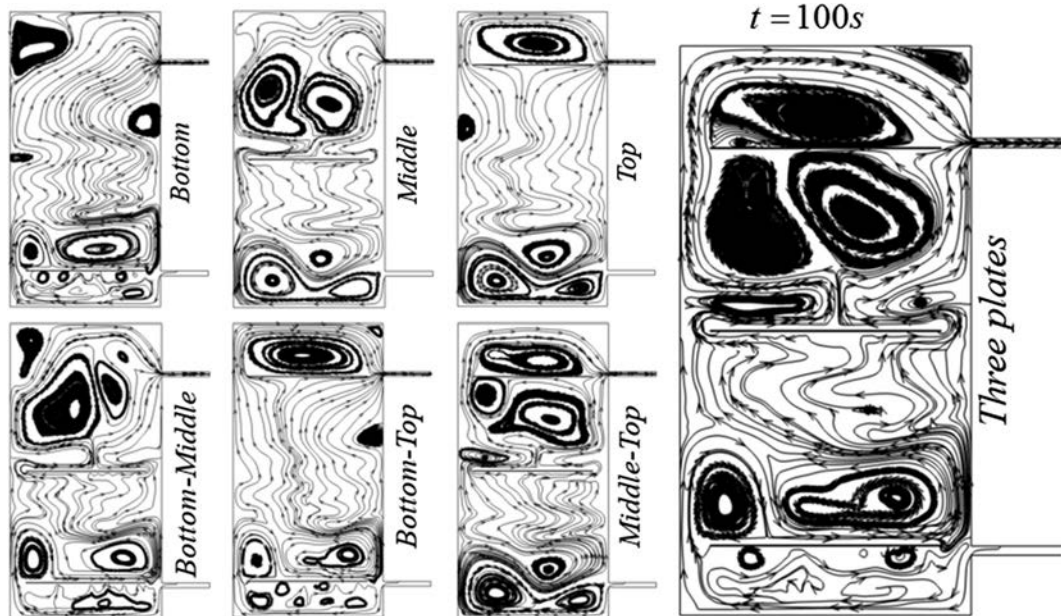


Fig. 10. Effect of flat plate at different positions on streamlines (Configuration A).

It is seen from Fig. 10, that a secondary recirculation zone is formed at the top of the tank which prevents the warm uprising fluid to reach the top of the tank and hence a temperature incursion is formed there. By placing the flat plate in the middle or the top positions, the secondary recirculation is diminished and the center of the main circulation moves upward and becomes closer to the tank wall. For these two cases, the bottom region of the tank is occupied with a cold and relatively motionless fluid.

4.1.2. Configuration B with different orientations

Fig. 11 depicts the temperature contours of charging process for different flat plates angles ranging from 0° to 180° at $t = 100$ s. In this configuration, the tank height and diameter are constants and have values of 800 mm and 400 mm respectively to illustrate the required effect of flat plates integration. The cold flow enters the tank from bottom surface and the hot flow exits the tank from the top surface. The outlet flow has high momentum energy and the inlet cold water diffuses inside the tank and causes mixing flow on the top layers. In addition, the inlet jet flow strikes the opposite wall with significant impingement effect at high aspect ratio that affects the flow structure inside the storage tank. The results show that the flat plate inclinations have a significant effect on the temperature stratification during the charging process. As we can observe, the tank with flat plate inclination of $\alpha = 0^\circ$ is providing homogeneous temperature stratification. The case of $\alpha = 30^\circ$ is charging fast compared to other cases where the jet flow from water bottom inlet strikes the flat plate wall as shown in Fig. 11. As a result, the flow temperature near the top wall is slightly high compared to other locations. For the same time, the flow structure on the top of the tank is almost the same for the cases of $\alpha = 0^\circ$ and $\alpha = 45^\circ$. Accordingly, the thermal stratification develops rapidly towards the exit port at $\alpha = 120^\circ$ because the water temperature increases significantly in time.

The streamlines distribution inside the tank at $t = 60$ s for different flat plates inclinations is illustrated in Fig. 12. The solution has non symmetrical flow characterized by different counter-cells due to the non symmetry of boundary conditions. Some cells rotate in the direction of clockwise and the others rotates in the opposite direction for all flat plate's inclinations: $\alpha = 0^\circ, \alpha = 30^\circ, \alpha = 45^\circ$ and $\alpha = 120^\circ$. When we change the angle of the flat plate, the intensity of the recirculation within the tank increases and the centers of the streamlines move upward. Moreover, the flow is also characterized by the development of the circular rollers in both storage tank bottom and top positions. As the

hot fluid flow is initiated through the bottom port inlet, the tank cold fluid adjacent to the interface of the flat plate is progressively heated and flows upward due to the buoyancy force. The uprising warm fluid in the tank around the vicinity of the tank wall impinges to the top horizontal wall and turns towards the centerline of the tank and hence pushes the cold fluid to drop down around the centerline. As a result, a recirculation zone is formed at the tank bottom and top regions as may be seen in Fig. 12. As time elapses, the warm fluid at the top region is replaced with the warmer fluid, and pushes down the previously warm fluid layer, causing the development of a stable thermal stratification. The lower part of the tank is occupied with an almost stagnant cold fluid.

4.2. Tank outlet and average temperatures evolution

The evolution of the average tank temperature as well as the hot water outlet temperature for different plate position's which are inserted into the tank are presented in Fig. 13. These two performance indicators decrease as a function of time, due to the cold water charge supplied and which replaces the volume of the hot water consumed. The use of a single plate at the middle, at the top and their middle-top combination does not greatly influence the two parameters mentioned above. On the other hand, the use of three plates inside the tank improves the average temperature by only one degree from the instant $t = 200$ s. Moreover, the temperature of the pulsed hot water is disturbed from time $t = 225$ s because of the additional number of obstacles (the combined influence of the plate at the bottom and the plate at the top), if we compare it with the three other studied cases.

4.3. Temperature distribution along the tank height

The evolution of the temperature along the vertical axis of the storage tank (z axis) according to three lines (line 1, line2 and line 3) is presented in Fig. 14. This indicator describes the temperature longitudinal variation for three positions as a function of time: for a plate inserted at the bottom, for two plates inserted at the middle and at the top and finally for three plates inserted at the bottom, middle and at the Top of the tank.

In both cases, lines 1 and 3 are used to measure the axial temperature changes between the end of the plate and the inner wall of the tank, while line 2 represents the measurement of the temperature evolution along the axis of the cylindrical tank. For the last case, three

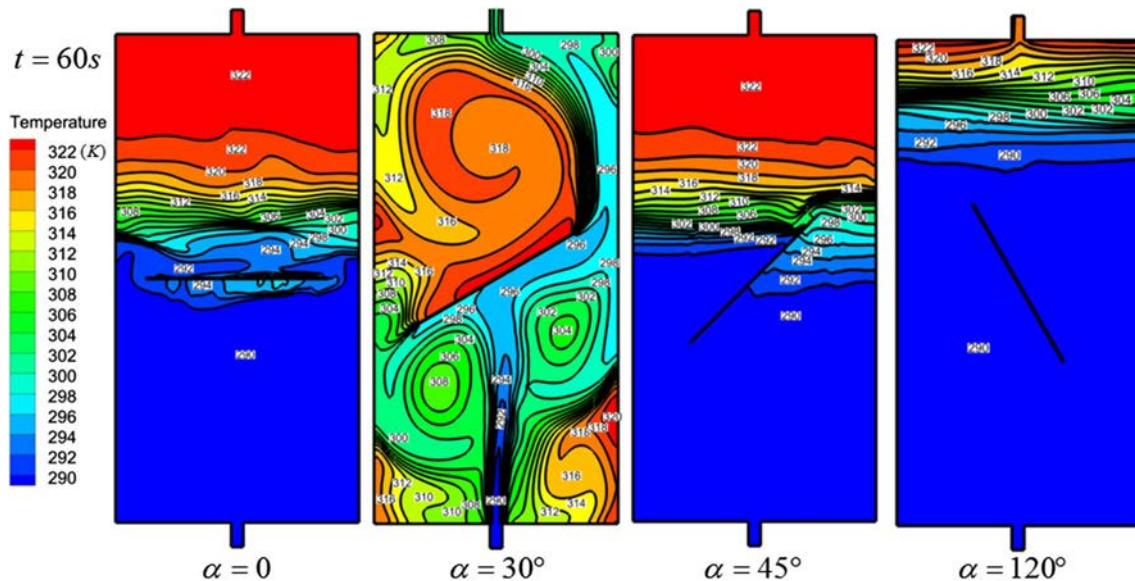


Fig. 11. Effect of flat plate orientations on temperature contours (Configuration B).

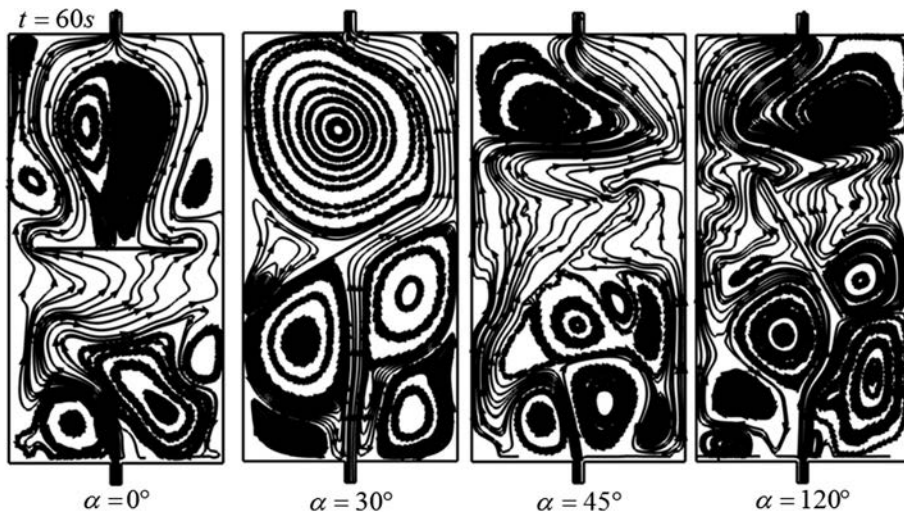


Fig. 12. Effect of flat plate orientations on streamlines (Configuration B).

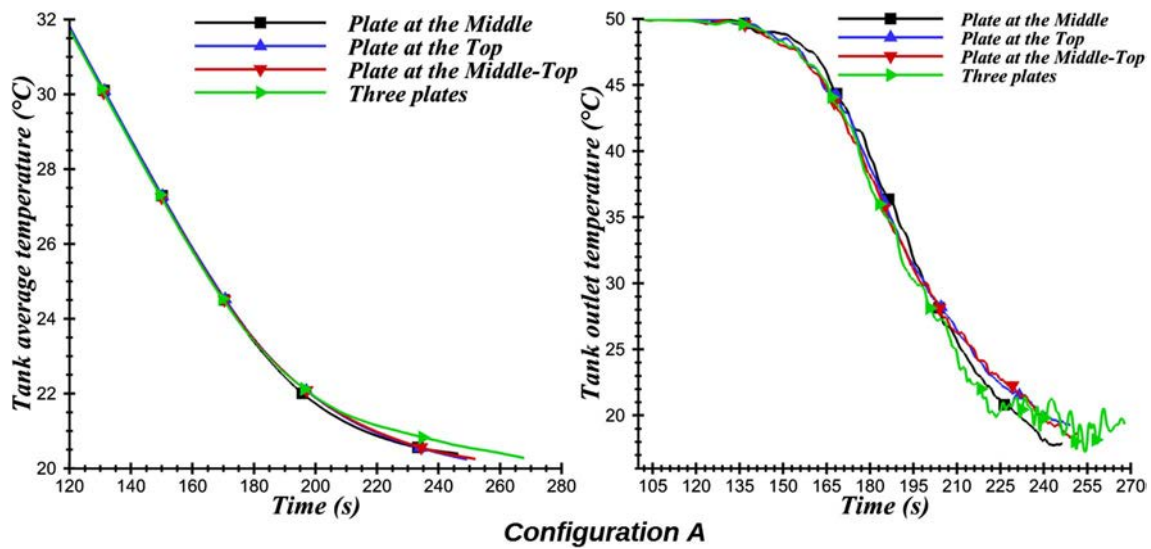


Fig. 13. Effect of flat plate positions on temperature evolution (Configuration A).

plates were inserted inside the tank, line 1 is used to measure the temperature between the end of the plates and the internal surface of the tank. The two lines 2 and 3 measure the evolution of the axial temperature between the two plates inserted at the middle and at the top respectively.

The configuration with two plates localized at the middle and the top delay the mixing of layers of laminated water that mixes with the cold water charged. Contrary to the configuration that involves a single plate at the bottom tank, where the thermocline is quickly destroyed. The use of three plates and two plates preserve the extended thermocline for a duration of 250 s as presented in Fig. 14.

4.4. Richardson number

The Richardson number is an important parameter that governs the fluid flow and it is extensively used to describe stratification in hot water storage tank (Castell et al., 2010). The Richardson number is a measure of the ratio of buoyancy forces to mixing forces, which is expressed by:

$$Ri = \frac{g\beta H(T_{top} - T_{bottom})}{V_{in}^2} \quad (14)$$

As can be seen, a beneficial thermal stratification can be realized for $Ri > 1$. The evolution of the Richardson number for the two

configurations A and B is presented in Fig. 15. The trends of this indicator are strongly affected by the position, number, and the plates orientations. The Figures compare the evolution of Richardson number as discharging progressed for the two configurations. For the configuration A, the arrangement of two Middle-Top plates presents a Richardson number whose evolution is more stable (between the two values 1.8 and 4.5) as a function of time in the interval [50 s; 250 s]. As observed, a smaller Richardson number is obtained at $t = 150$ s which is implying a lower degree of thermal stratification. This can be explained by the fact that the flow pattern in vertical tank is influenced by mixing forces. In this case, mixing forces are more pronounced due to the existing of two recirculation zones. Regarding the configuration B, a horizontal plate located in the middle of the tank ($\alpha = 0$) is optimal, because the Richardson number is minimal and decreases to 1 over the interval [15 s; 100 s].

4.5. Stratification number

4.5.1. Configuration A with different positions

The stratification number is an adimensional number used to characterize stratification inside a vertical storage tank (Abdelhak et al., 2015). This important parameter could effectively evaluates the thermal behavior of the storage tank in the discharging process. Thus, to get more detailed information on the development of thermal

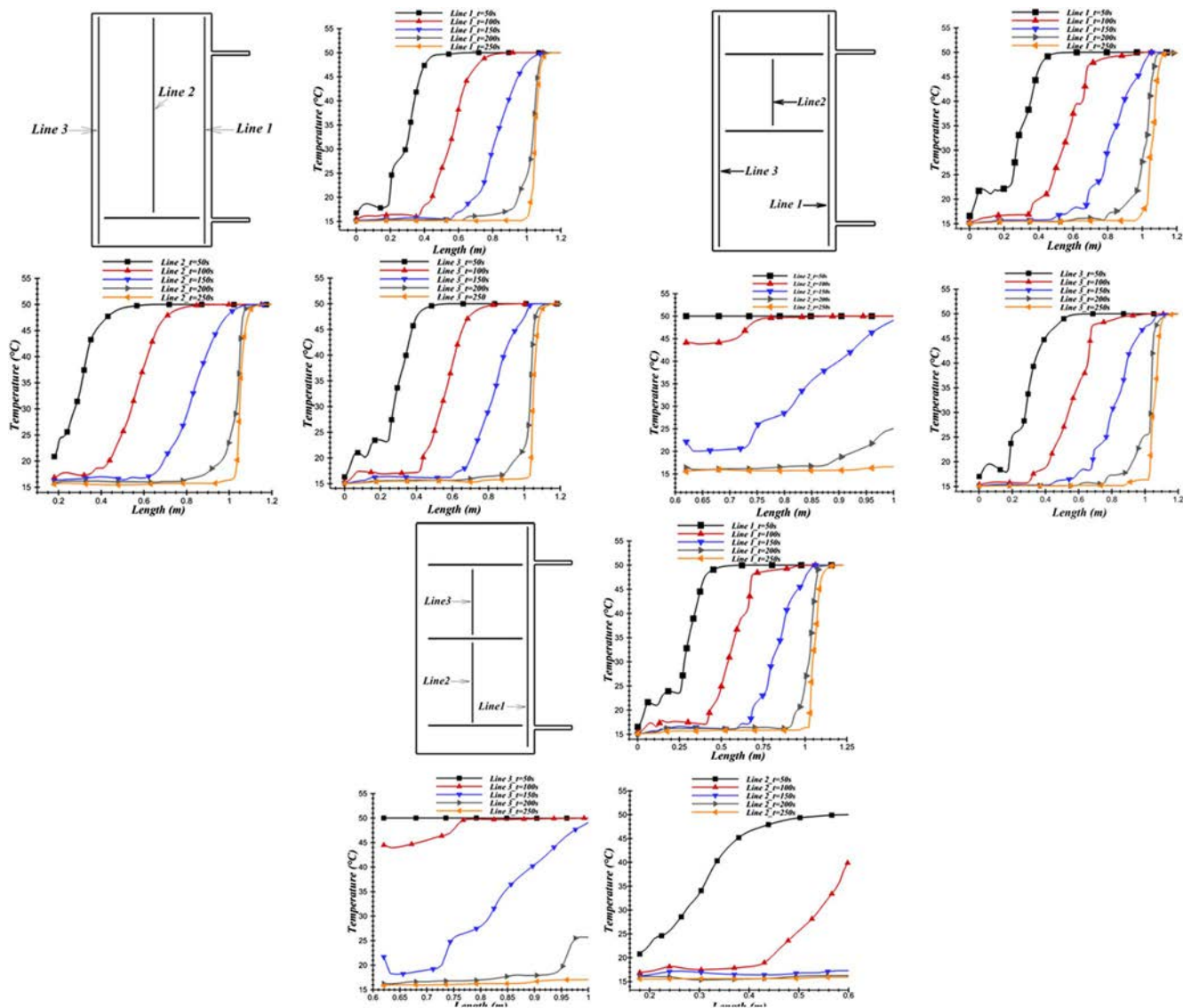


Fig. 14. Temperature distribution along the tank height for different axis lines.

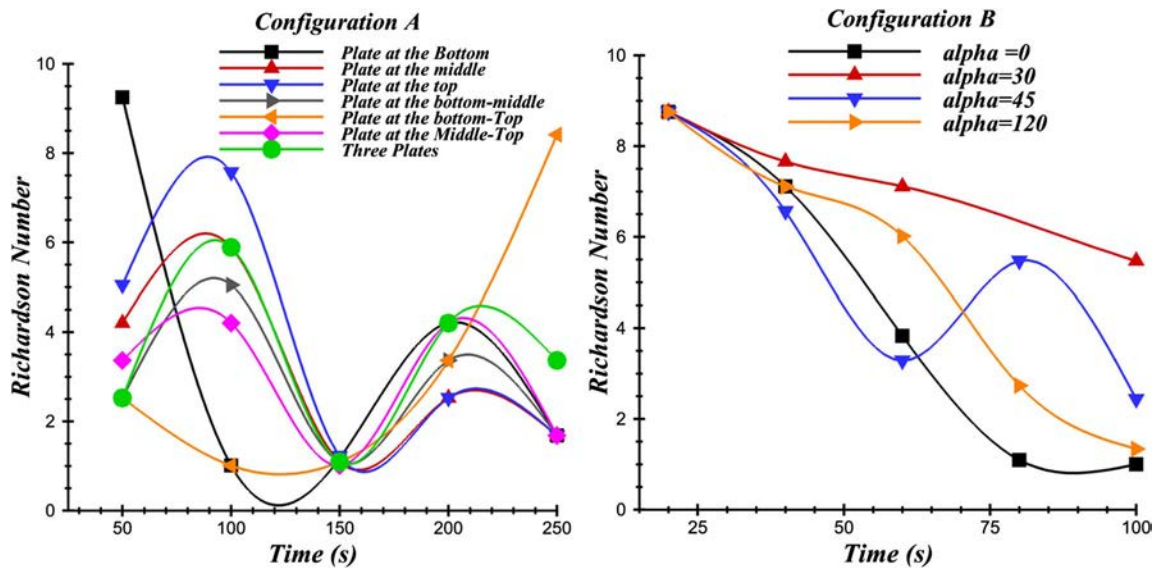


Fig. 15. Effect of flat plate on Richardson number for both configurations A and B.

stratification for both the studied configurations, the stratification number expressed as the ratio of the mean of the transient temperature gradients to the maximum mean temperature gradient for the charging and discharging processes was used, as expressed by Eq. (15):

$$Str(t) = \frac{\left(\frac{\partial T}{\partial z}\right)_t}{\left(\frac{\partial T}{\partial z}\right)_{max}} \quad (15)$$

$$\left(\frac{\partial T}{\partial z}\right)_t = \frac{1}{J-1} \sum_{j=1}^{J-1} \left(\frac{T_{j+1}-T_j}{\Delta z}\right) \quad (16)$$

$$\left(\frac{\partial T}{\partial z}\right)_{max} = \frac{T_{max}-T_{in}}{(J-1)\Delta z} \quad (17)$$

The racking applied flow makes the discharging time of the tank lasting 250 s. For this reason, the stratification number evolution was assessed during this period. The stratification number Str is calculated during this study at two different positions $z = H/2$ and $z = 3H/4$ to predict the effect of flat plate position on the degree of stratification inside the storage tank. Figs. 16 presents the evolution of the Str over a period of 250 s for $z = H/2$ and $z = 3H/4$ respectively.

The evolution of the Stratification number indicator as a function of time for two precise localizations located at $z = 3H/4$ and $z = H/2$ of the configuration A is presented in Fig. 16. It is in our interest to keep a maximum lamination number during the charging/discharging operation to ensure optimum thickness of the thermocline. This indicator is influenced by the difference in the local temperature varying along the axis of the vertical tank and the minimum temperature of the water to be charged. For the height $z = 3H/4$, the flat plate located at the middle top configuration performs best during the 200 s operating cycle, as this indicator is maximum and remains above other configurations. Concerning the height $z = H/2$ which is the midpoint of the tank. We note that the flat plate at the middle configuration improves the thermocline better in comparison with the remaining configurations. This localization $z = H/2$ demonstrates the contribution of different arrangement of the plates inserted in the improvement of the tank lamination. Nevertheless, it's interesting to keep a good stratification close to the point where the hot water extraction is carried out ($z = 3H/4$). Reason why the insertion of two plates at the Middle-Top level of the configuration A is the most optimal in relief with the other studied cases.

For $z = H/2$ (Fig. 16), and during the discharging mode ($t < 150$ s), the middle configuration has a Str greater than the remaining configurations. It decreases from its maximum value 1 to 0.1. After 150 s ($150 < t < 200$ s), the middle-top configuration optimizes the

stratification number, followed by both three-plates and bottom configurations. In the last quarter time ($200 < t < 250$ s), the flat plate located at the middle position maintains Str at its value of 0.08. This configuration is followed by the others cases including Bottom-top and top plates.

Concerning $z = 3H/4$ (Fig. 16), three intervals of the Str evolution during the drawing time of the hot water are distinguished. For $50 < t < 100$ s, the bottom-top configuration is optimal. It is followed by the two others configurations, i.e, middle-top and three-plates. For $100 < t < 200$ s, the effect of the position is taking place. The bottom-top configuration optimizes Str which is followed by the middle and then the top configuration. On the last interval ($200 < t < 250$ s), we notice that the instant $t = 200$ s represents an inflection point for the Str for both configurations middle and middle-top. Indeed, the Str increases from 0.2 to 0.3. This number in the middle-top, bottom-middle, three-plate and bottom-top configurations continues to decrease to take the final value of 0.05. The stratification speed for the middle-top configuration is slower than the remaining ones. We conclude that for $z = 3H/4$, the middle configuration optimizes Str during the hot water discharging mode.

4.5.2. Configuration B with different orientations

Stratification number evolution as a function of time for configuration B is presented in Fig. 17. This indicator was evaluated for a point located at height of $z = 3H/4$. The inclination of the $\alpha = 30^\circ$ plate optimizes the Stratification number over an operating time spanning equal to 80 s. Indeed, it operates within a margin between 0.65 and 0.85.

5. Conclusion

The major purpose of this study is to develop CFD numerical framework in order to assess thermal stratification in vertical solar storage tanks, which is a device mainly used in solar water heating systems. First of all, the used CFD code was validated against a literature experimental results and a good agreement was found. Thereafter, two main storage tank's configurations were studied. The main difference between Configuration A and B was the position of the nozzles from which the charge and discharge operation occurs, in addition to the number of flat plates integrated inside the tanks, their positions and their tilt angle.

A set of performance indicators were defined to carry out this CFD numerical performance assessment, such as temperature and streamlines contours, Richardson and stratification numbers, and eventually the hot water temperature to load and the temperature evolution in

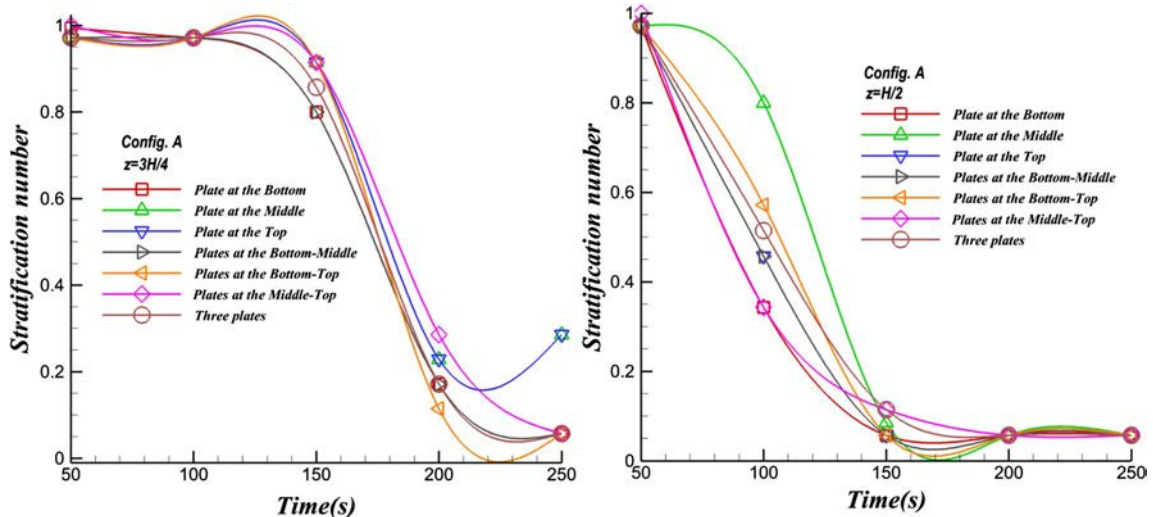


Fig. 16. Effect of flat plate at different positions on Stratification number for $z = \frac{H}{2}$ and $z = \frac{3H}{4}$ (Configuration A).

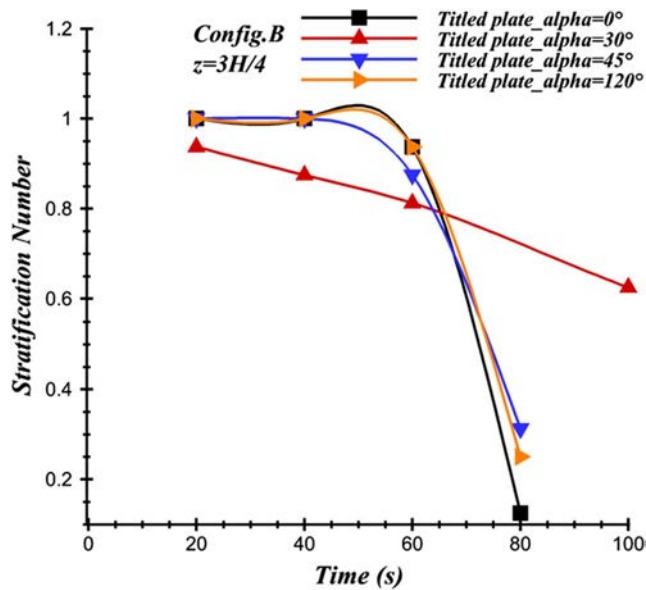


Fig. 17. Effect of flat plate for plate's different angles on Stratification number for $z = \frac{3H}{4}$ (Configuration B).

some specific areas where the thermocline is important to describe.

The major findings of the current analysis were that the tank with two plates located at the Middle and Top is the optimum case for configuration A, and the tank with a 30° tilted plate is offering the best performance for the configuration B, because the thermocline extent and the stratification number values were important, and finally a Richardson number which is greater than 1, which means that the buoyancy forces overcome the mixing forces. All in all, our numerical simulation results served to analyze the flow characteristics and the thermal stratification performance during charging and discharging phases for two vertical storage tanks configurations.

Acknowledgment

The authors would like to express their appreciation and to acknowledge the financial support received for this work from the "Institut de Recherche en Energie Solaire et Energies Nouvelles" (IRESEN-Morocco) under the projects of Solar Cooling Process in Morocco (SCPM) and SOL'R SHERMSY.

References

Abdelhak, O., Mhiri, H., Bournot, P., 2015. Cfd analysis of thermal stratification in domestic hot water storage tank during dynamic mode. In: *Building Simulation*. Springer, pp. 421–429.

Adolfo, C., Moreira, G.A., Zeghamati, B., Leite, A.P., 2014. Numerical analysis of a thermal storage tank as part of a 20 kW solar/gas adsorption air conditioning system. *Energy Proc.* 57, 2600–2608. <http://dx.doi.org/10.1016/j.egypro.2014.10.271>. 2013 ISES Solar World Congress. <<http://www.sciencedirect.com/science/article/pii/S1876610214016385>>.

Ali, T., Bakar, R.A., Sup, B.A., Zainudin, M.F., Ming, G.L., 2015. Study on thermal-fluid effect of thermal energy storage tank design in solar energy applications. *Energy Proc.* 68, 3–11. <http://dx.doi.org/10.1016/j.egypro.2015.03.226>. 2nd International Conference on Sustainable Energy Engineering and Application (ICSEEA) 2014 Sustainable Energy for Green Mobility. <<http://www.sciencedirect.com/science/article/pii/S1876610215005329>>.

Allouche, Y., Varga, S., Bouden, C., Oliveira, A.C., 2016. Validation of a {CFD} model for the simulation of heat transfer in a tubes-in-tank {PCM} storage unit. *Renew. Energy* 89, 371–379. <http://dx.doi.org/10.1016/j.renene.2015.12.038>. <<http://www.sciencedirect.com/science/article/pii/S0960148115305401>>.

Altuntop, N., Arslan, M., Ozceyhan, V., Kanoglu, M., 2005. Effect of obstacles on thermal stratification in hot water storage tanks. *Appl. Therm. Eng.* 25, 2285–2298. <http://dx.doi.org/10.1016/j.applthermaleng.2004.12.013>. <<http://www.sciencedirect.com/science/article/pii/S1359431105000311>>.

Bonanos, A., Votyakov, E., 2016. Sensitivity analysis for thermocline thermal storage tank design. *Renew. Energy* 99, 764–771. <http://dx.doi.org/10.1016/j.renene.2016.07.052>. <<http://www.sciencedirect.com/science/article/pii/S096014811630667X>>.

Brown, N., Lai, F., 2011. Enhanced thermal stratification in a liquid storage tank with a porous manifold. *Solar Energy* 85, 1409–1417. <http://dx.doi.org/10.1016/j.solener.2011.03.024>. <<http://www.sciencedirect.com/science/article/pii/S0038092X11001071>>.

Cascetta, M., Cau, G., Puddu, P., Serra, F., 2016. A comparison between {CFD} simulation and experimental investigation of a packed-bed thermal energy storage system. *Appl. Therm. Eng.* 98, 1263–1272. <http://dx.doi.org/10.1016/j.applthermaleng.2016.01.019>. <<http://www.sciencedirect.com/science/article/pii/S1359431116000740>>.

Castell, A., Medrano, M., Solé, C., Cabeza, L., 2010. Dimensionless numbers used to characterize stratification in water tanks for discharging at low flow rates. *Renew. Energy* 35, 2192–2199. <http://dx.doi.org/10.1016/j.renene.2010.03.020>. <<http://www.sciencedirect.com/science/article/pii/S0960148110001370>>.

Dragsted, J., Furbo, S., Dannemand, M., Bava, F., 2017. Thermal stratification built up in hot water tank with different inlet stratifiers. *Solar Energy* 147, 414–425. <http://dx.doi.org/10.1016/j.solener.2017.03.008>. <<http://www.sciencedirect.com/science/article/pii/S0038092X1730169X>>.

Erdemir, D., Altuntop, N., 2016. Improved thermal stratification with obstacles placed inside the vertical mantled hot water tanks. *Appl. Therm. Eng.* 100, 20–29. <http://dx.doi.org/10.1016/j.applthermaleng.2016.01.069>. <<http://www.sciencedirect.com/science/article/pii/S1359431116300199>>.

Fan, J., Furbo, S., 2012. Thermal stratification in a hot water tank established by heat loss from the tank. *Solar Energy* 86, 3460–3469. <http://dx.doi.org/10.1016/j.solener.2012.07.026>. <<http://www.sciencedirect.com/science/article/pii/S0038092X12002897>>.

Gandhi, M.S., Joshi, J.B., Nayak, A.K., Vijayan, P.K., 2013. Reduction in thermal stratification in two phase natural convection in rectangular tanks: {CFD} simulations and {PIV} measurements. *Chem. Eng. Sci.* 100, 300–325. <http://dx.doi.org/10.1016/j.ces.2013.02.064>. 11th International Conference on Gas-Liquid and Gas-Liquid-Solid Reactor Engineering. <<http://www.sciencedirect.com/science/article/pii/S0009250913002224>>.

García-Marí, E., Gasque, M., Gutiérrez-Colomer, R.P., Ibáñez, F., González-Altozano, P., 2013. A new inlet device that enhances thermal stratification during charging in a hot water storage tank. *Appl. Therm. Eng.* 61, 663–669. <http://dx.doi.org/10.1016/j.applthermaleng.2013.08.023>. <<http://www.sciencedirect.com/science/article/pii/S1359431113006042>>.

Gasque, M., González-Altozano, P., Maurer, D., Moncho-Esteve, I.J., Gutiérrez-Colomer, R.P., Palau-Salvador, G., García-Marí, E., 2015. Study of the influence of inner lining material on thermal stratification in a hot water storage tank. *Appl. Therm. Eng.* 75, 344–356. <http://dx.doi.org/10.1016/j.applthermaleng.2014.10.040>. <<http://www.sciencedirect.com/science/article/pii/S1359431114009119>>.

Göppert, S., Lohse, R., Urbaneck, T., Schirmer, U., Platzer, B., Steinert, P., 2009. New computation method for stratification pipes of solar storage tanks. *Solar Energy* 83, 1578–1587. <http://dx.doi.org/10.1016/j.solener.2009.05.007>. <<http://www.sciencedirect.com/science/article/pii/S0038092X09001170>>.

Gross, G., Vogel, H., Wippermann, F., 1987. Dispersion over and around a steep obstacle for varying thermal stratification—numerical simulations. *Atmos. Environ.* 21 (1967), 483–490. [http://dx.doi.org/10.1016/0004-6981\(87\)90031-X](http://dx.doi.org/10.1016/0004-6981(87)90031-X). <<http://www.sciencedirect.com/science/article/pii/000469818790031X>>.

Gyüre, B., János, I.M., 2003. Stratified flow over asymmetric and double bell-shaped obstacles. *Dyn. Atmos. Oceans* 37, 155–170. [http://dx.doi.org/10.1016/S0377-0265\(03\)00030-7](http://dx.doi.org/10.1016/S0377-0265(03)00030-7). <<http://www.sciencedirect.com/science/article/pii/S0377026503000307>>.

Haller, M.Y., Yazdandshenas, E., Andersen, E., Bales, C., Streicher, W., Furbo, S., 2010. A method to determine stratification efficiency of thermal energy storage processes independently from storage heat losses. *Solar Energy* 84, 997–1007. <http://dx.doi.org/10.1016/j.solener.2010.03.009>. <<http://www.sciencedirect.com/science/article/pii/S0038092X10001131>>.

Jin, S., Chen, L., Bu, G., 2017. Experimental investigation of a novel multi-tank thermal energy storage system for solar-powered air conditioning. *Appl. Therm. Eng.* <http://dx.doi.org/10.1016/j.applthermaleng.2017.05.160>. <<http://www.sciencedirect.com/science/article/pii/S1359431117317386>>.

Jordan, U., Furbo, S., 2005. Thermal stratification in small solar domestic storage tanks caused by draw-offs. *Solar Energy* 78, 291–300. <http://dx.doi.org/10.1016/j.solener.2004.09.011>. {ISES} Solar World Congress 2003. <<http://www.sciencedirect.com/science/article/pii/S0038092X04002841>>.

Joseph, J., Agrawal, G., Agarwal, D.K., Pisharady, J., Kumar, S.S., 2016. Effect of insulation thickness on pressure evolution and thermal stratification in a cryogenic tank. *Appl. Therm. Eng.* <http://dx.doi.org/10.1016/j.applthermaleng.2016.07.015>. <<http://www.sciencedirect.com/science/article/pii/S1359431116311449>>.

Kaloudis, E., Grigoriadis, D., Papanicolaou, E., 2016. Numerical simulations of constant-influx gravity currents in confined spaces: application to thermal storage tanks. *Int. J. Therm. Sci.* 108, 1–16. <http://dx.doi.org/10.1016/j.ijthermalsci.2016.04.018>. <<http://www.sciencedirect.com/science/article/pii/S1290072915300259>>.

Kassemi, M., Kartuzova, O., 2016. Effect of interfacial turbulence and accommodation coefficient on cfd predictions of pressurization and pressure control in cryogenic storage tank. *Cryogenics* 74, 138–153. <http://dx.doi.org/10.1016/j.cryogenics.2015.10.018>. 2015 Space Cryogenics Workshop, June 24–26, 2015, Phoenix, AZ Hosted by NASA Glenn Research Center, Cleveland, OH, USA. <<http://www.sciencedirect.com/science/article/pii/S0011227515001447>>.

Kong, L., Yuan, Weixing, Zhu, N., 2016. {CFD} simulations of thermal stratification heat storage water tank with an inside cylinder with openings. *Proc. Eng.* 146, 394–399. <http://dx.doi.org/10.1016/j.proeng.2016.06.419>. The 8th international cold climate {HVAC} Conference. <<http://www.sciencedirect.com/science/article/pii/S187705816308827>>.

Meng, Z., Zhang, P., 2017. Experimental and numerical investigation of a tube-in-tank latent thermal energy storage unit using composite {PCM}. *Appl. Energy* 190,

- 524–539. <http://dx.doi.org/10.1016/j.apenergy.2016.12.163>. <<http://www.sciencedirect.com/science/article/pii/S0306261916319432>>.
- Miana, M., Cantín, O., Millán, C., Valdés, J.R., Bernad, C., Sánchez, J.M., 2011. Enhancement of the thermal design of bitumen emulsion tanks by scale analysis, {CFD} models and experimental tests. *Appl. Energy* 88, 4106–4112. <http://dx.doi.org/10.1016/j.apenergy.2011.03.026>. <<http://www.sciencedirect.com/science/article/pii/S0306261911001966>>.
- Nash, A.L., Badithela, A., Jain, N., 2017. Dynamic modeling of a sensible thermal energy storage tank with an immersed coil heat exchanger under three operation modes. *Appl. Energy* 195, 877–889. <http://dx.doi.org/10.1016/j.apenergy.2017.03.092>. <<http://www.sciencedirect.com/science/article/pii/S0306261917303343>>.
- Rahman, A., Smith, A.D., Fumo, N., 2016. Performance modeling and parametric study of a stratified water thermal storage tank. *Appl. Therm. Eng.* 100, 668–679. <http://dx.doi.org/10.1016/j.applthermaleng.2016.01.163>. <<http://www.sciencedirect.com/science/article/pii/S135943111630117X>>.
- Reddy, K., Jawahar, V., Sivakumar, S., Mallick, T., 2017. Performance investigation of single-tank thermocline storage systems for {CSP} plants. *Solar Energy* 144, 740–749. <http://dx.doi.org/10.1016/j.solener.2017.02.012>. <<http://www.sciencedirect.com/science/article/pii/S0038092X17301056>>.
- Saghi, H., Lakzian, E., 2017. Optimization of the rectangular storage tanks for the sloshing phenomena based on the entropy generation minimization. *Energy* 128, 564–574. <http://dx.doi.org/10.1016/j.energy.2017.04.075>. <<http://www.sciencedirect.com/science/article/pii/S0360544217306412>>.
- Tay, N., Bruno, F., Belusko, M., 2012. Experimental validation of a cfd model for tubes in a phase change thermal energy storage system. *Int. J. Heat Mass Transfer* 55, 574–585. <http://dx.doi.org/10.1016/j.ijheatmasstransfer.2011.10.054>. <<http://www.sciencedirect.com/science/article/pii/S001793101100634X>>.
- Votyakov, E., Bonanos, A., 2015. Algebraic model for thermocline thermal storage tank with filler material. *Solar Energy* 122, 1154–1157. <http://dx.doi.org/10.1016/j.solener.2015.10.047>. <<http://www.sciencedirect.com/science/article/pii/S0038092X15006003>>.
- Wang, S., Davidson, J.H., 2015. Selection of permeability for optimum performance of a porous tube thermal stratification manifold. *Solar Energy* 122, 472–485. <http://dx.doi.org/10.1016/j.solener.2015.09.018>. <<http://www.sciencedirect.com/science/article/pii/S0038092X15005022>>.
- Wang, S., Davidson, J.H., 2017. Performance of a rigid porous-tube stratification manifold in comparison to an inlet pipe. *Solar Energy* 146, 298–308. <http://dx.doi.org/10.1016/j.solener.2017.02.045>. <<http://www.sciencedirect.com/science/article/pii/S0038092X17301469>>.
- Wang, Z., Zhang, H., Dou, B., Huang, H., Wu, W., Wang, Z., 2017a. Experimental and numerical research of thermal stratification with a novel inlet in a dynamic hot water storage tank. *Renew. Energy* 111, 353–371. <http://dx.doi.org/10.1016/j.renene.2017.04.007>. <<http://www.sciencedirect.com/science/article/pii/S0960148117303002>>.
- Wang, Z., Zhang, H., Dou, B., Zhang, H.H.G., 2017b. The thermal stratification characteristics affected by a novel equalizer in a dynamic hot water storage tank. *Appl. Therm. Eng.* <http://dx.doi.org/10.1016/j.applthermaleng.2017.06.045>. <<http://www.sciencedirect.com/science/article/pii/S1359431116332902>>.
- Yee, C., Lai, F., 2001. Effects of a porous manifold on thermal stratification in a liquid storage tank. *Solar Energy* 71, 241–254. [http://dx.doi.org/10.1016/S0038-092X\(01\)00043](http://dx.doi.org/10.1016/S0038-092X(01)00043). <<http://www.sciencedirect.com/science/article/pii/S0038092X01000433>>.
- Zachár, A., Farkas, I., Szlivka, F., 2003. Numerical analyses of the impact of plates for thermal stratification inside a storage tank with upper and lower inlet flows. *Solar Energy* 74, 287–302. [http://dx.doi.org/10.1016/S0038-092X\(03\)00188-9](http://dx.doi.org/10.1016/S0038-092X(03)00188-9). <<http://www.sciencedirect.com/science/article/pii/S0038092X03001889>>.